Frontiers of Information Technology & Electronic Engineering
www.jzus.zju.edu.cn; engineering.cae.cn; www.springerlink.com
ISSN 2095-9184 (print); ISSN 2095-9230 (online)
E-mail: jzus@zju.edu.cn

# Design of omnidirectional rydberg atomic sensors loaded with electric field enhancement structure using characteristic mode analysis

Zhenke DING†, Yi LIU†‡, Bo WU, Kai YANG, Ruibing RAN, Yi LIN, Yunqi FU

*College of Electronic Science and Technology, National University of Defense Technology, Changsha 410073, China.*

†E-mail: dingzhenke@nudt.edu.cn; yi_liu@nudt.edu.cn

Received Aug. 10, 2024; Revision accepted Mar. 4, 2025; Crosschecked

Unedited

**Abstract:** The integration of electric field enhancement structures (EFES) with Rydberg atomic sensors (RASs) has garnered considerable interest due to their potential to enhance detection sensitivity in quantum measurement systems. Despite this, there is a dearth of research on the directional response of EFES, and the analysis of the three-dimensional (3D) patterns of RAS remains a formidable challenge. RASs are employed in non-destructive measurement techniques and are responsive to electric fields, primarily serving as reception devices. However, analyzing their reception patterns is a complex task that requires a sophisticated approach. To address this, we have adopted characteristic mode (CM) analysis to illustrate on the omnidirectional performance of RAS. According to CM theory, the reception pattern can be calculated by a series of modal currents and their corresponding coefficients. The analytical representation of these coefficients negates the need for time-consuming full-wave (FW) numerical simulations, which are typically required to generate EFES patterns due to the necessity of scanning numerous angle parameters. This approach significantly reduces the complexity of solving EFES patterns and provides insightful guidance for the design process. To validate the efficacy of our proposed method, we constructed three prototypes. The results indicate that the final model resonates at 1.96GHz, achieving an electric field gain of 25dB and an out-of-roundness of 2.4dB. These findings underscore the effectiveness of our method for analyzing EFES patterns, highlighting its potential for future applications in the field.

**Key words:** Rydberg atomic sensor; Characteristic mode; Electric field enhancement structure.
https://doi.org/10.1631/FITEE.2400700 **CLC number:**

## 1 Introduction

Quantum precision measurement technology based on quantum theory provides a novel pathway for measuring physical parameters. This technology has the characteristic of self-calibration and enables the absolute measurement of physical quantities (Sedlacek et al., 2012). Over the past decade, researchers have been exploring its application of the technology in microwave electric field measurement, with the most typical being Rydberg atom-based electric field measurement technology (Sedlacek et al., 2012, 2013; Holloway et al., 2014; Yang et al., 2022; Zhang et al., 2023). The theoretical detection sensitivity of microwave electric field measurement based on quantum theory is higher than that of traditional electronic microwave measurement systems (Fan et al., 2015). However, there is still a significant gap between the measurement values of the detection sensitivity and the theoretical values (Dixon et al., 2023; Mao et al., 2023; Zhang et al., 2023; Yuan et al., 2024; Sandidge et al., 2024).

Rydberg atom-based microwave electric field measurement principles provide avenues for improving detection sensitivity, with two main approaches emerging: quantum optical methods (Bussey et al.,

‡ Corresponding author
© Zhejiang University Press 2025

2021; Liu et al., 2022; Yang et al., 2023b) and microwave methods (Wu et al., 2022, 2023; Yang et al., 2023c; Holloway et al., 2022). Recent advancements in microwave methods, including heterodyne detection (Simons et al., 2021; Yao et al., 2022), modulation signals (Meyer et al., 2018; Song et al., 2019; Holloway et al., 2019; Jiao et al., 2019; Yang et al., 2023a), multi-channel detection (Robinson et al., 2021; Hu et al., 2023), and loaded with electric field enhancement structures (EFESs) (Sandidge et al., 2024; Yang et al., 2023c; Holloway et al., 2022) have shown promise in improving the detection sensitivity of Rydberg atom-based systems. The EFESs act as a special boundary condition added to the Rydberg atomic sensors (RASs), thereby altering the electric field response of the sensors to incident waves. EFES can enhance the electric field in a specific area, thus improving detection sensitivity. It should be noted that the difference between the RASs and antennas is that RASs respond to the electric field in space rather than capturing the electromagnetic power density. Therefore, the RASs do not to prioritize impedance matching for receiving microwave but rather concentrate on the degree of electric field enhancement.

One of the influencing factors of the directional response of the RASs is the direction of the incident electric field. It is necessary for RAS to study directionality to meet the different application requirements. Consequently, the EFES pattern should be defined as electric field amplitude gain (E-Gain) pattern. An omnidirectional pattern is commonly used for directional finding applications (Ren, 2022; Choi and Sarabandi, 2018). Researchers have found that the response of RASs to incident waves is approximately isotropic(Yuan et al., 2024; Anderson et al., 2021; Mao et al., 2023), meaning that RASs are similar to the dipole antennas with good omnidirectional performance. Currently, few scholars have studied the EFES's response to incident waves from different directions. While using EFES enhances detection sensitivity, it could potentially impact the omnidirectional performance of the sensors. Balancing the E-Gain and the omnidirectional performance of the sensors is a challenge

Furthermore, RASs cannot be used for radiation applications in the current research stage. This means that when studying the directional response of the EFES, we cannot obtain its radiation pattern and reception pattern through port excitation based on the reciprocity theorem. The EFES pattern solution is similar to solving the scattering problem of a near-field electric field. RAS is an electric field probe close to EFES under microwave incident. The current analysis approach requires configuring angle parameters in full-wave (FW) simulation software to acquire reception patterns via parameter scanning. The measurement method follows the same approach. It costs too much calculation time to complete pattern design and optimization. However, there is no better way to obtain the reception pattern of the EFES. Most of the current research papers only explored the E-Gain for EFES at the fixed incident angle (Yang et al., 2023c; Anderson et al., 2018; Holloway et al., 2022). Therefore, researching directionality analysis methods for the EFES is of great significance in improving the sensitivity of Rydberg atom probes in microwave electric field measurement.

In a word, EFES is a special boundary condition for RASs. The directional response of EFES is consistent with that of the integration sensors. Typically, EFES is composed of metal and dielectric, which is generally similar to an SRR Holloway et al. (2022). The sensors can be simply considered as a glass bubble filled with air in the electromagnetic wave propagation. In the field of antennas, by analyzing the modal currents on the metal surface through the characteristic mode (CM) theory Harrington and Mautz (1971), it is possible to control the radiation or scattering modes and calculate the classical circuit parameters Manteuffel et al. (2022); Adams et al. (2022); Huang et al. (2018); Chen and Wang (2015); Grundmann and Manteuffel (2021); Shi et al. (2023); Dicandia and Genovesi (2023); Zhang et al. (2022). Meanwhile, in CM theory, CMs are independent with external sources, and the EFES is a passive structure without feed-ports. CM theory may be suitable for guiding EFES design. Only the external source contains the parameters related to incident angle in the E-Gain patterns. Based on the CM theory, the EFES pattern can be expressed as the product of a set of modal electric field and corresponding coefficients. The modal electric field depends on the external source and the corresponding coefficients can be calculated analytically, reducing the complexity of the solution. Therefore, we believe that applying CM theory to the design of EFES a wise and feasible solution. We will analyze

Unedited

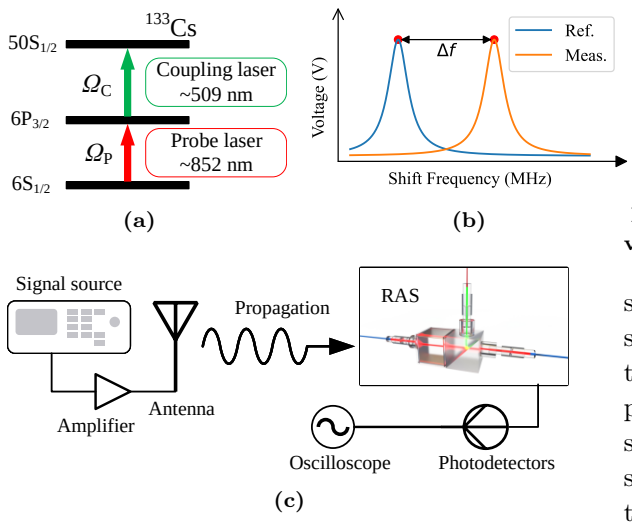


**Fig. 1: (a)Overview of experimental energy diagram; (b)the diagram of the AC-Stark frequency shift; (c)the sketch of the atom experimental setup.**

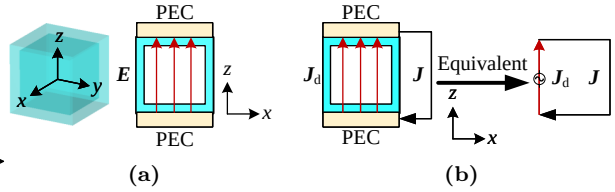


**Fig. 2: (a) The atomic cell and expected electric field view; (b) the equivalent current model**

the patterns by examining the EFES modal currents based on CM theory. It could provide a clear physical explanation and a better design method for EFES just like guiding antenna design.

In this paper, a novel pattern analysis method for RAS with EFES proposed by calculating the CMs of the EFES. Section 2 describes the Rydberg atom-based electric field measurement principles and E-Gain pattern analysis method based on CM theory. Section 3 analyzes the method of controlling the omnidirectional performance of RASs. Section 4 validates the effectiveness of the proposed method and verifies the pattern control effect through experiments. Section 5 part summarizes this paper.

## 2 Analysis of the mode pattern

### 2.1 Basic theory for Rydberg atom electric field measurement

Fig.1(a) shows that the two-photon Rydberg electromagnetically induced transparency (EIT) ladder scheme. There are two laser resources: one with a power of 14.6mW at 510nm and the other with 8.3$\mu$W at 852nm. The 852nm laser is locked to one of the $6S_{1/2} \rightarrow 6P_{3/2}$ transitions with a Rabi frequency $\Omega_p$. Similarly, the 510 nm laser is locked to the $6P_{3/2} \rightarrow 50S_{1/2}$ transitions with a Rabi frequency $\Omega_c$. The EIT signal is then detected by a photodetector. When the radio-frequency (RF) resource is turned off, the EIT signal only has one peak, similar to the blue line in Fig. 1(b). When the RF is turn on and the power is limited, the EIT signal will produce the AC Stark shift. The blue line will be shift to the orange line Cardman et al. (2020). The spectral shift $\Delta f$ between the two peaks is related to the electric field magnitude $|E|$ and can be expressed as Cardman et al. (2020)

$$\Delta f = -\frac{1}{4}\alpha E^2 \tag{1}$$

where the $\alpha$ is called as the dynamic scalar polarizability. Fig.1(c) shows the experimental setup overview. The sensor is same as the Wu et al. (2024) and Mao et al. (2023) as shown in Fig. 1(c). An oscilloscope is used to measured the EIT signals received by a photodetector.

### 2.2 The current distribution for the enhanced electric field

According to the measurement theory of RASs Sedlacek et al. (2012), it is expected that there is a strong electric field in the atomic cell center of RAS, and the polarization should be consistent with the polarization of the optical path, which is typically $+\boldsymbol{e}_z$. To avoid the distribution of the electric field with zero points like $TE_{30}$, the direction of the electric field in the cell should be the same. Therefore, it is recommended that adding PEC condition on the cell of $z_{\max}$ and $z_{\min}$ face enhances the electric field as shown in Fig. 2(a). According to current continuity equation Harrington (2001), it can be expressed as

$$\boldsymbol{J}_{\mathrm{d}} = \frac{\partial \boldsymbol{D}}{\partial t} = \varepsilon \frac{\partial \boldsymbol{E}}{\partial t} \tag{2}$$

$$\nabla \cdot (\boldsymbol{J} + \frac{\partial \boldsymbol{D}}{\partial t}) = 0 \tag{3}$$

where $\boldsymbol{J}_{\mathrm{d}}$, $\boldsymbol{D}$, $\boldsymbol{E}$, $t$ and $\varepsilon$ represent displacement current density, electrical flux density, electric field, time and dielectric constant, respectively. EFES converts

Unedited

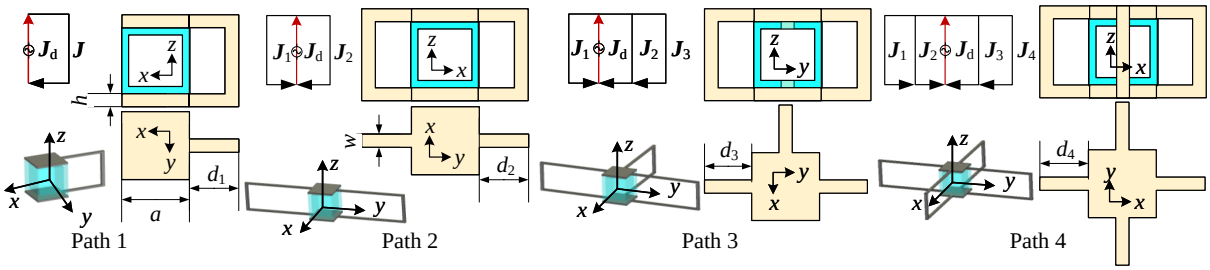


**Fig. 3: The equivalent current model and corresponding physical structure. Four models are named Path 1, 2, 3, and 4. $d_1$=14; $d_2$=27.4; $d_3$=34.3; $d_4$=38.8; $w$=1; $h$=0.5; $a$=10.(unit=mm)**

weak electromagnetic waves in space into a localized enhanced electric field, leading to the presence of enhanced displacement current $J_d$ in the region where the electric field is enhanced. Therefore, a metallic conductor is needed between the upper and lower plates to carry conduction current. It can also be regarded as the resonant current model of the SRR.

Therefore, a current model is proposed as shown in Fig. 2(b). A conduction current can be achieved by connecting two metal nodes outside the PEC boundaries. When $J$ as shown in Fig. 2(b) is constructed by only one conduction current, the most typical EFES model is named as Path 1 as shown in Fig. 3. The current distributions in Wu et al. (2024, 2023); Holloway et al. (2022) are also consistent with Path 1. Based on this current model and simple rotational symmetry, we can propose models with more conduction current paths as shown in Fig. 3. To understand the operating mechanism of the proposed structure, the intrinsic CMs supported by the structure are investigated using CM analysis.

### 2.3 The Resonance CMs of the EFES

When a RAS is loaded with EFES, the electric field at the center position of the atomic cell is an important parameter for analysis. The E-Gain is defined as the amplitude of the electric field at the atom cell center point under the excitation of a unit amplitude uniform plane wave.

To realize the proposed current model and study the corresponding pattern, the CM theory is introduced for analysis. According to CM theory Chen and Wang (2015), the electric field $\boldsymbol{E}(r_i)$ at any one point $r_i$ can be represented by a set of orthogonal CM electric fields $E_m$ as

$$\boldsymbol{E}(\boldsymbol{r}_i) = \sum^{m} a_m \boldsymbol{E}_m(r_i) = \sum^{m} \frac{< \boldsymbol{E}_{\text{inc}}, \boldsymbol{J}_m >}{1 + \mathrm{j}\lambda_m} \boldsymbol{E}_m(\boldsymbol{r}_i) \tag{4}$$

$$a_m = \frac{< \boldsymbol{E}_{\text{inc}}, \boldsymbol{J}_m >}{1 + \mathrm{j}\lambda_m} \tag{5}$$

$$\text{MS} = \frac{1}{|1 + \mathrm{j}\lambda_m|} \tag{6}$$

where $a_m$, MS, $\boldsymbol{J}_m$, $\boldsymbol{E}_m(\boldsymbol{r}_i)$, $\lambda_m$, and $\boldsymbol{E}_{\text{inc}}$ represent the modal weighting coefficients (MWC), the modal significant (MS), the $m$th modal current density, the $m$th modal electric field at the $r_i$ point, the $m$th eigenvalue, and the incident electric field, respectively. It should be noted that MS is an intrinsic property representing the coupling capability of each CM with external sources.

### 2.4 The pattern for EFES using CM theory

To study the directional response between incident electric field $E_{\text{inc}}$ and the EFES, a uniform plane wave is used as the incident wave. A unit uniform plane wave $\boldsymbol{E}_{\text{inc}}$ propagating in any direction can be expressed as

$$\boldsymbol{E}_{\text{inc}} = \boldsymbol{E}_{\text{amp}} \mathrm{e}^{-\mathrm{j}\boldsymbol{k}\cdot\boldsymbol{r}} \tag{7}$$

$$\begin{aligned} \boldsymbol{E}_{\text{amp}} = {} & \boldsymbol{e}_x(\cos\theta\cos\varphi\cos\alpha - \sin\varphi\sin\alpha) \\ & + \boldsymbol{e}_y(\cos\theta\sin\varphi\cos\alpha + \cos\varphi\sin\alpha) \\ & - \boldsymbol{e}_z(\sin\theta\cos\alpha) \end{aligned} \tag{8}$$

$$\boldsymbol{k} = (\boldsymbol{e}_x \sin\theta\cos\varphi + \boldsymbol{e}_y \sin\theta\sin\varphi + \boldsymbol{e}_z \cos\theta)k \tag{9}$$

$$\boldsymbol{r} = \boldsymbol{e}_x x + \boldsymbol{e}_y y + \boldsymbol{e}_z z \tag{10}$$

where $\boldsymbol{E}_{\text{amp}}$, $\boldsymbol{k}$, $k$, and $\boldsymbol{r}$ represent the electric field amplitude vector, wave vector, phase constant, and propagation vector, respectively. $\alpha$ represents the rotation angle of the electric field vector relative to the $\boldsymbol{x}$-axis and $\varphi$, and $\theta$ represents the spherical

Unedited

angle of the incident plane wave. According to Eqs. (6)-(9), the unit uniform incident plane wave vector $\boldsymbol{E}_{\text{inc}}$ can be expressed as

$$\boldsymbol{E}_{\text{inc}} = \boldsymbol{E}(\alpha, \varphi, \theta, k) \tag{11}$$

The EFES pattern $G(\alpha, \varphi, \theta)$ is defined as

$$G(\alpha, \varphi, \theta) = \frac{\boldsymbol{E}_1(r_i)}{\boldsymbol{E}_0(r_i)} \tag{12}$$

where $\boldsymbol{E}_1(\boldsymbol{r}_i)$, $\boldsymbol{E}_0(\boldsymbol{r}_i)$ represent the electric field in the atom cell with and without EFES, respectively. Substituting Eq.(7) into Eq.(4), the electric field at any one point can be written as

$$\boldsymbol{E}(\boldsymbol{r}_i) = \sum^{m} \frac{< \boldsymbol{E}(\alpha, \varphi, \theta, k), \boldsymbol{J}_m >}{1 + \mathrm{j}\lambda_m} \boldsymbol{E}_m(r_i) \tag{13}$$

$\boldsymbol{J}_m$, $\lambda_m$, and $\boldsymbol{E}_m(\boldsymbol{r}_i)$ can be calculated by one CM analysis, and these parameters are only related to structure parameters. Substituting Eq.(13) into Eq.(12), the E-Gain $G(\alpha, \varphi, \theta)$ is expressed as

$$G(\alpha, \varphi, \theta) = \frac{\sum^{m} \frac{<\boldsymbol{E}(\alpha,\varphi,\theta,k),\boldsymbol{J}_m>}{1+\mathrm{j}\lambda_m} \boldsymbol{E}_m(\boldsymbol{r}_i)}{\boldsymbol{E}_0(r_i)} \tag{14}$$

Eq.(14) implies that the pattern of the EFES can be calculated through a single CM analysis. Traditional analysis methods typically require multiple times FW simulations by scanning parameters, resulting in a computation of the three-dimensional (3D) directional pattern for $n \times m \times l$ sampling points, where $n$, $m$, $l$ represent the number of sampled points for $\alpha$, $\varphi$, and $\theta$. By contrast, the proposed method reduces the computation to a single CM analysis, significantly reducing the simulation time compared with traditional methods. Combined with CM theory, it provides a convenient method of analysis from a new perspective. Moreover, it allows for controlling the angle stepping accuracy by manipulating variables. Compared with the antennas, the RASs detect the electric field amplitude rather than the electromagnetic power. Therefore, the directionality $D$ for EFES should be expressed as

$$D = \frac{4\pi |E|_{\max}}{\int_0^{2\pi} \mathrm{d}\varphi \int_0^{\pi} E(\theta, \varphi) \sin\theta \mathrm{d}\theta} \tag{15}$$

This Eq.(15) could be used to evaluate the directionality of the EFES.

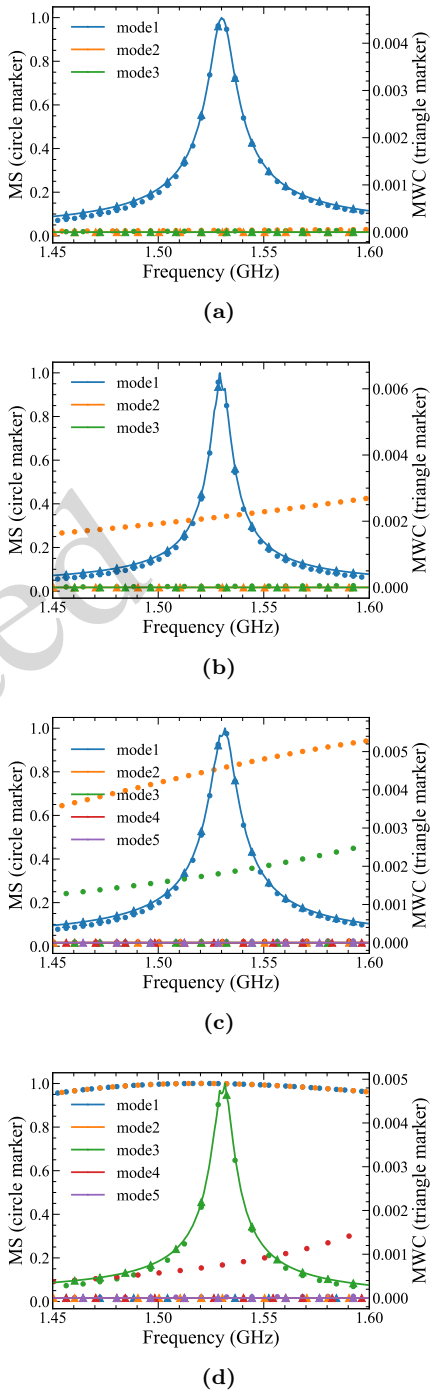


**Fig. 4: The MSs and MWCs for four models (a) the MSs and MWCs for Path 1; (b) the MSs and MWCs for Path 2; (c) the MSs and MWCs for Path 3; (d) the MSs and MWCs for Path 4.**

## 3 Pattern analysis based on CM theory

### 3.1 Raw model structures for pattern snalysis

However, the proposed current distribution model in Fig. 3 still requires verification to deter-

Unedited

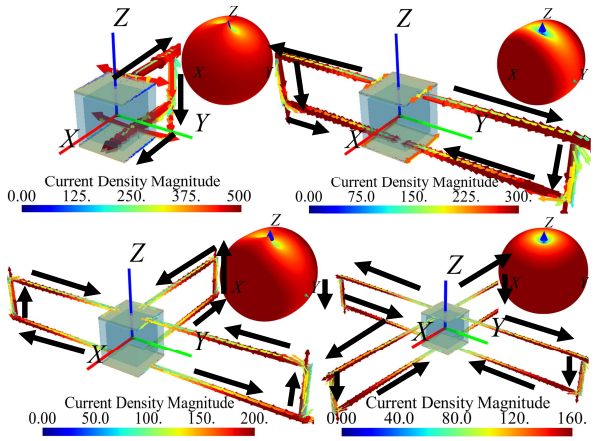


**Fig. 5: The modal current and corresponding 3D-view pattern calculated by the CM method at 1.53GHz.**

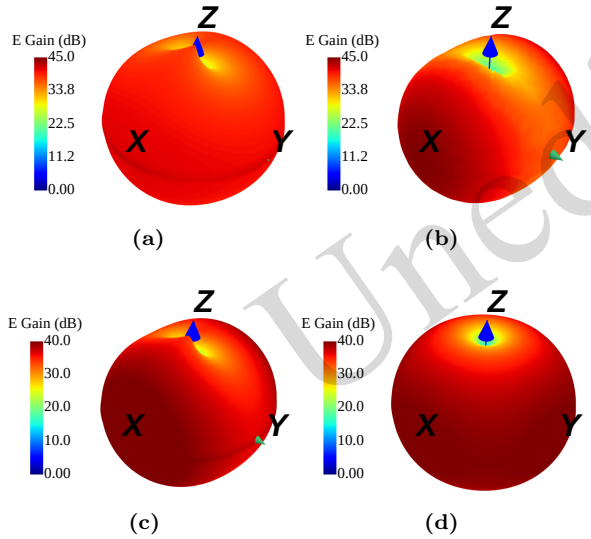


**Fig. 6: The 3D-view pattern calculated by FW simulation. (a)Path 1; (b)Path 2; (c)Path 3; (d)Path 4.**

mine its consistency with reality. To quickly verify this theory, the metal material is set as a PEC, and the dielectric material is set as an ideal dielectric with a dielectric constant of 4.2. The resonant frequencies of the four models are the same. Fig. 4 shows that the CM analysis for the above four models, as shown in Fig. 2(c). The excitation source is a uniform plane wave with unit amplitude, and incident in the $-\boldsymbol{e}_x$ direction ($\theta = 90°, \varphi = 0°$). The MS results show that the number of the mode satisfying MS>0.707 increases with the increment of the current path number.

However, the MWC results show that only one mode is excited by the plane wave for each model, concluding that the analyzed models operate in a

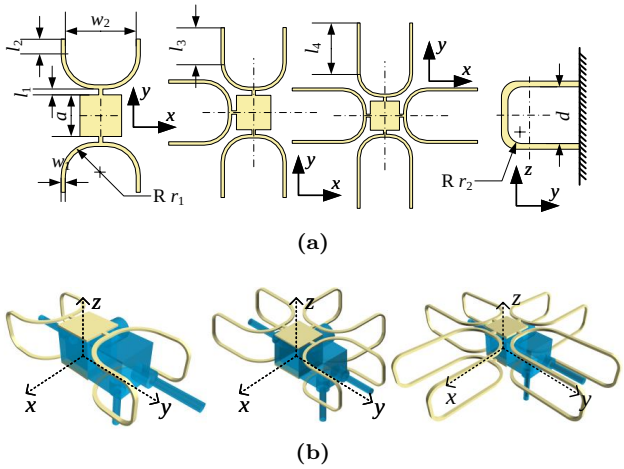


**Fig. 7: The configuration of the proposed three models. The metal thickness is 0.5mm. (a)The sturcure of the models; (b)the 3D views of the models. $l_1$=1; $l_2$=7; $l_3$=13.3; $l_4$=20.4; $w_1$=1; $w_2$=17; $r_1$=7; $r_2$=3; $d$=10.(unit=mm)**

single mode. Fig. 5 shows the modal current distribution with the highest MWC value for each model and the corresponding pattern was calculated using Eq.(14). The modal current distribution is consistent with Fig. 3. Fig. 6 shows the calculated and FW simulated patterns for four models. The patterns of four models are analyzed using Eq.(14) and compared with the FW simulated results. The results calculated by CM method and FW simulation are similar, indicating that the CM method can be used to analyze the E-Gain pattern of the EFES. The Wu et al. (2024) presents an EFES with a curent distribution similar to Path 1, where the patterns are also similar.

### 3.2 The improved structure for pattern analysis

The Wu et al. (2024) specifically verified the model with only one current path. This paper verified the accuracy of the proposed method in models with 2, 3, and 4 current paths. The initial design of the structure did not consider the RAS structure that needed to be loaded. Thus, improvements were made to the structures named IP 2, 3, and 4, as shown in Fig 7. The blue material represents the RAS and the yellow material represents copper. Fig. 8 shows that the CM analysis for the proposed models. To further reveal the coupling degree between patterns and plane wave source, we will select the largest mode of MWC, which is the mode most ex-

Unedited

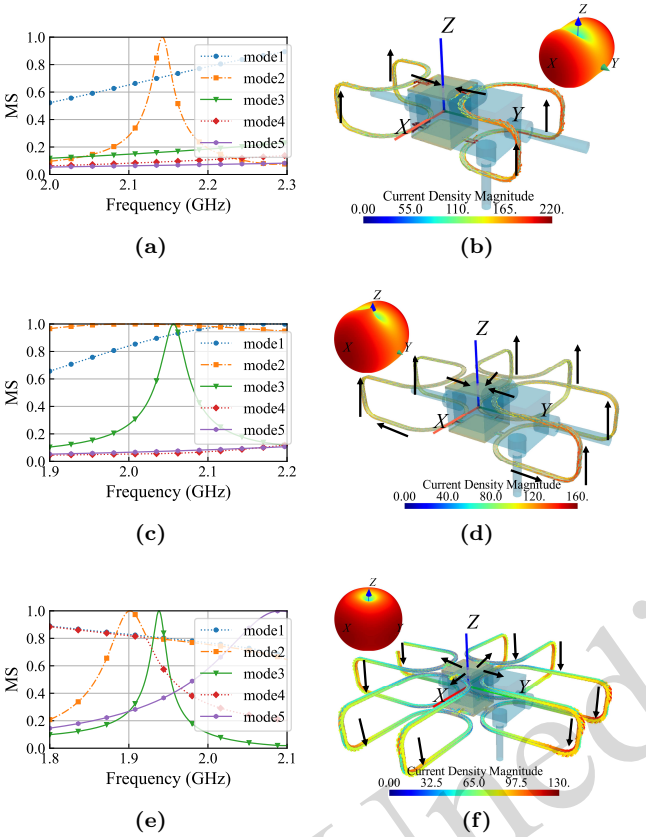


**Fig. 8: The MSs and MWCs for four models (a) the MSs for IP 2; (b) The mode 2 current and patterns of IP2 at 2.15GHz. (c) the MSs for IP 3; (d) The mode 3 current and patterns of IP3 at 2.08GHz. (e) the MSs for IP 4; (f) The mode 3 current and patterns of IP4 at 1.96GHz.**

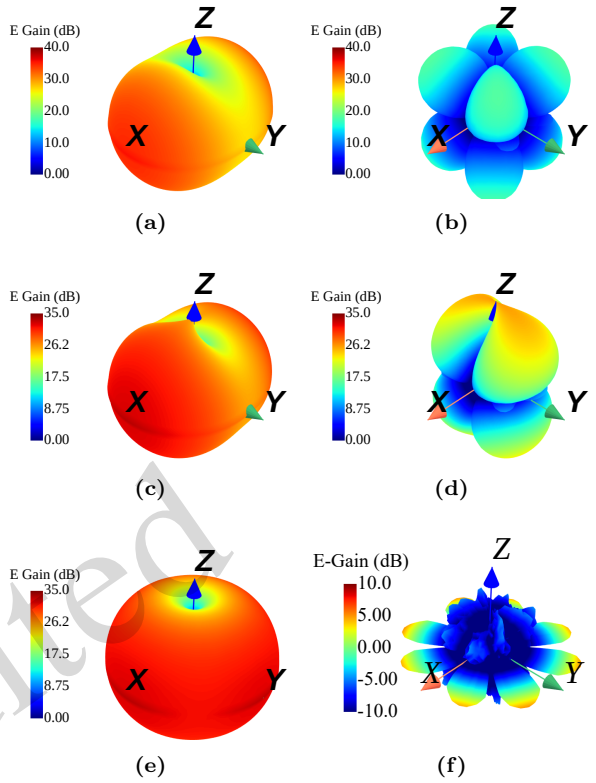


**Fig. 9: The 3D-view reception pattern of each model calculated by FW simulated. (a)the copolar of pattern IP2 at 2.15GHz; (b)the crosspolar pattern of IP2 at 2.15GHz; (c)the copolar of pattern IP3 at 2.08GHz; (d)the crosspolar pattern of IP3 at 2.08GHz; (e)the copolar of pattern IP4 at 1.96GHz; (f)the crosspolar pattern of IP4 at 1.96GHz.**

Unedited

cited by the plane wave source. Fig. 8 shows that the largest MWC modal currents and the corresponding patterns for each model, calculated using Eq.(14). The modal currents show that the direction of currents is consistent with the proposed theory in Fig. 3.

To verify the results of the CM, we simulated the proposed models in CST software. Fig. 9 shows that the copolar and crosspolar reception pattern of each model. The results of the FW simulation were obtained by scanning the incident angle of the plane wave source around the spherical surface. The scanning angles d$\varphi$ and d$\theta$ are 5°, and then they are interpolated to 1° using an interpolation algorithm. It can be observed that the omnidirectionality of the pattern increases with the addition of the path. Table 1 shows that the directionality of the IP series was calculated by Eq.(14). The omnidirectional performance increases with the increase in the path number. This is because the path represents the modal current and extending in path leads to a more uniform spatial distribution of current, resulting in a more uniform electric field response in the atomic cell center of RAS. It is evident that the patterns calculated based on the CM theory are similar to the shape of the FW simulated. This is a good indication that the proposed method based on the CM theory can guide the pattern design of the EFES. Furthermore, using this method requires only a single calculation for CMs to obtain the pattern, reducing the optimization time for pattern design.

**Table 1: Comparison of the directionality of the IP series models**

| Model | IP2 | IP3 | IP4 | Probe |
|---|---|---|---|---|
| FW simulation (dB) | 2.94 | 2.47 | 1.63 | 1.96 |
| CM method (dB) | 2.46 | 1.73 | 1.12 | None |

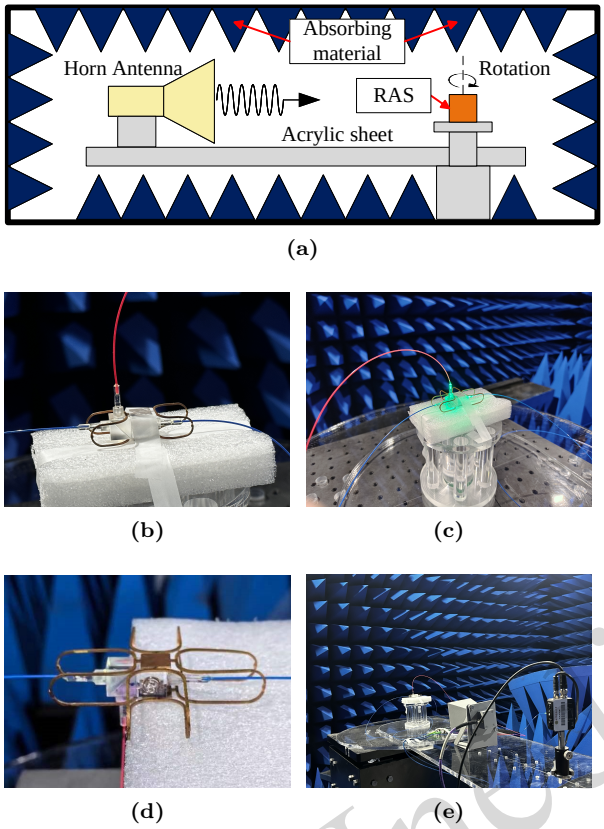


**Fig. 10: Photograph of the fabricated prototypes and measurement scene. (a)the atom reception pattern measurement system diagram; (b)the photograph of the IP2; (c)the photograph of the IP3; (d)the measurement scene of the IP4; (e) the measurement scene of all.**

## 4 Measurement and discussion

To validate the proposed design method and operating mechanism, the three models were fabricated and measured. Fig. 10 shows the fabricated prototypes and measurement scene. First, it is necessary to explain the measurement steps of the experiment results. The first thing to note is the frequency response curve of the E-Gain. The measurement steps are similar to those outlined by Yang et al. (2023c). The measurement step details are as follows: (1)Connect the experimental instruments with EFES as shown in Fig. 1(c); (2)open the RF resource and set a high level microwave power such as 10 dBm, and define the scanning frequency range and step; (3)Traverse each frequency point while recording the shift $\Delta f$, and then plot a line showing the relationship between the $\Delta f$ and the source power named curve 1; (4)remove the EFES structure, set the RF source frequency to the peak frequency of curve 1, and then

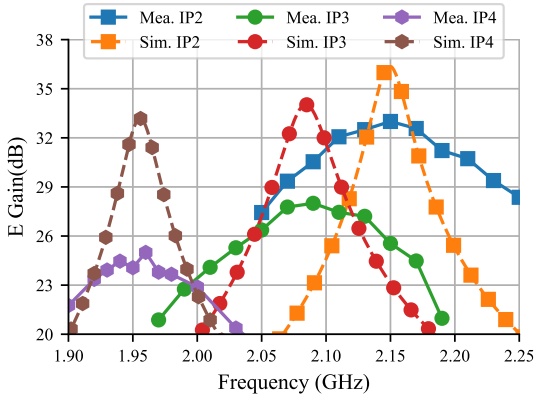


**Fig. 11: The simulated and measured frequency response curves for three models.**

adjust the RF power to match the spacing with the peak shift $\Delta f_{\max}$; (5)traverse each frequency point again to plot a relationship line named curve 2, as in Step 3. The power difference between curve 1 and 2 at the same frequency shift $\Delta f_0$ is the E-Gain. The frequency response curves can be obtained based on the relative relationship between variables.

Fig. 11 shows that the frequency response curves for the three proposed models. It can be seen that the maximum E-Gain of the measured results is lower than the simulated results. However, the 3dB-bandwidth of the measured results is larger than the simulated results. It indicates that the Q-values of the measured are smaller than the simulated and the loss of the measured is higher. The error is that the error originates from the losses caused by machining metal materials, which are greater compared to the simulation.

Next, it should be noted the measurement steps for the E-Gain pattern measurement setup. The measurement steps are similar to those outlined by Wu et al. (2024); Yuan et al. (2024). The measurement system refers to the construction of the antenna pattern measurement system as shown in Fig. 10(a). The measurement step details are as follows: (1)connect the experimental instruments with EFES as shown in Fig. 10(a); (2)set the RF source frequency to the corresponding structure resonant frequency and set a high-level microwave power, such as 10 dBm; (3)record the AC-stark shift $\Delta f$ as shown in Fig. 1(b); (4)rotate the antenna angle and repeat the Step 1 and 2 until a circle is completed.

Fig. 12 illustrates that the normalized E-Gain patterns. It is evident that the omnidirectional per-

Unedited

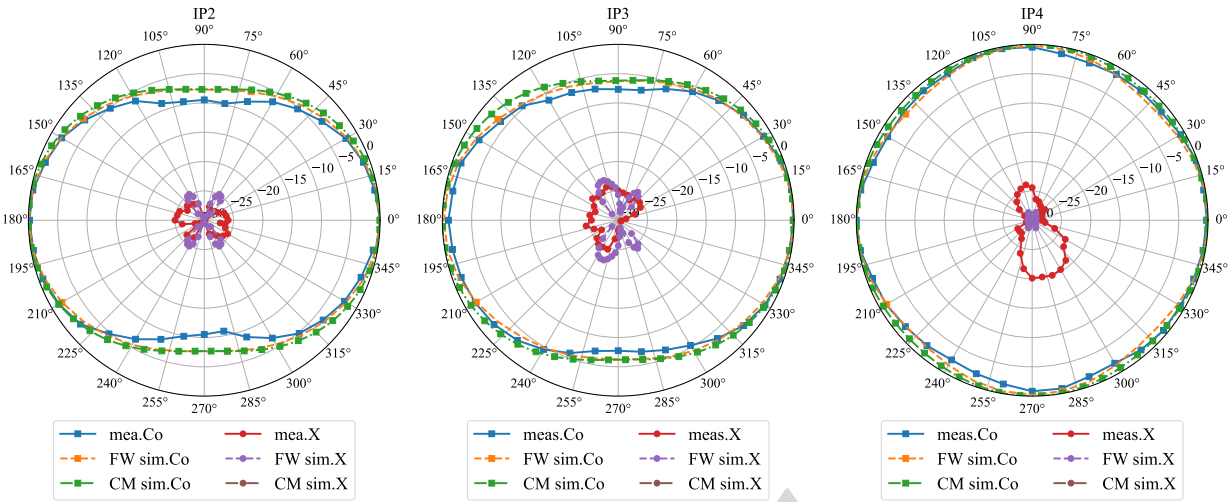


**Fig. 12: The simulated and measured normalized reception patterns for the three proposed prototypes ($\theta = 90°$).**

**Table 2: Performance comparison**

| Ref. | Mao et al. (2023) | Yuan et al. (2024) | Wu et al. (2024) | IP4 | IP3 | IP2 |
|---|---|---|---|---|---|---|
| Frequency(GHz) | 4.48 | 129.6, 4.8 | 2.06 | 1.96 | 2.08 | 2.15 |
| Out-of-roundness | 3.5 | 0.28, 2.5 | 7.8 | 2.4 | 8.8 | 10.7 |
| E-Gain | 0 | None | 21.5 | 25 | 27 | 33 |

*None: The reference article did not mention.

Unedited

formance of the proposed models improves with an increasing number of paths. The variation trends of the measured are consistent with those of the simulated for all models. Table 2 shows that some related papers similar to this works. This paper demonstrates a commendable ability to balance the E-Gain and out-of-roundness, resulting in achieved control over the pattern.

To verify whether the method is applicable to higher frequencies, we proportionally reduced the size of structure IP4 to half of its original dimensions and compared the results of the CM method and the FM method. As shown in the Fig.13, the resonant frequency of the changed structure is 4.032 GHz. The results from the CM method and the FM method match well, indicating that the method is suitable for higher frequencies.

Combining Eq.(4), the directivity of the structure is related to the incident wave source and the modal current. To simplify the model, we only discuss the situation where the structure is symmetric about the y-axis. At this time, the incident wave along the positive direction of the x-axis and the

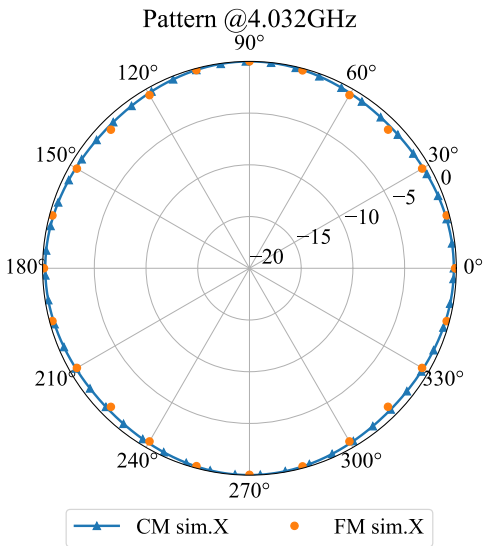


**Fig. 13: The pattern of the changed structure for verifying at higher frequency (4.032GHz)**

wave along the negative direction of the x-axis satisfy:

$$\boldsymbol{E}_{inc}^{+}(x) = -\boldsymbol{E}_{inc}^{-}(-x) \tag{16}$$

According to the analysis in the previous text, the model improved based on symmetry usually operates in a single mode, and it has an even symmetry in current, with the current satisfying:

$$\boldsymbol{J}_m(x) = -\boldsymbol{J}_m(-x) \tag{17}$$

Therefore, by combining Eq. (4), (16), and (17), we can obtain:

$$\begin{aligned}\boldsymbol{E} &= \sum^{m} \frac{< \boldsymbol{E}_{\text{inc}}^{+}(\boldsymbol{x}), \boldsymbol{J}_m(x) >}{1 + \mathrm{j}\lambda_m} \boldsymbol{E}_m(\boldsymbol{r}_i) \\ &= \sum^{m} \frac{< -\boldsymbol{E}_{\text{inc}}^{-}(-\boldsymbol{x}), \boldsymbol{J}_m(x) >}{1 + \mathrm{j}\lambda_m} \boldsymbol{E}_m(\boldsymbol{r}_i) \\ &= \sum^{m} \frac{< -\boldsymbol{E}_{\text{inc}}^{-}(-\boldsymbol{x}), -\boldsymbol{J}_m(-x) >}{1 + \mathrm{j}\lambda_m} \boldsymbol{E}_m(\boldsymbol{r}_i) \\ &= \sum^{m} \frac{< \boldsymbol{E}_{\text{inc}}^{-}(-\boldsymbol{x}), \boldsymbol{J}_m(-x) >}{1 + \mathrm{j}\lambda_m} \boldsymbol{E}_m(\boldsymbol{r}_i)\end{aligned} \tag{18}$$

From Eq.(18), it is evident that the responses of the two cases are the same. This indicates that by regulating the symmetry of the current, the response of the EFES can be changed, thereby achieving omnidirectional control of the EFES. When the current mode is asymmetric, the results from forward incidence and backward incidence lead to the same response, thus causing asymmetry in the pattern.

## 5 Conclusions

This paper proposes a pattern analysis method for RAS's pattern to design omnidirectional EFES based on CM theory. We derive new mathematical formulas for pattern analysis of EFES, which can be divided into modal currents and external sources. Modal currents are independent of external sources and represent an intrinsic property. The shape of modal patterns is determined by modal currents. Only the external source contains the pattern parameters related to the incident angle, which determines the weighting coefficients of each modal pattern in the total pattern. The proposed method guides the analysis and design of the EFES by separating parameters. According to the demand of the RASs, the EFES current models are proposed. The mechanism of the current models is analyzed through CM theory. The directionality of EFESs is changed bu controlling the current spatial distribution. The number of the current path increases and the symmetry of the structure enhances for the improvement of the RASs' omnidirectional performance. To validate the effectiveness of the proposed method, three prototypes were fabricated for measurement. The results indicated that IP4 achieves good omnidirectional performance and can enhance the detection sensitivity of the system. This indicates the proposed CM analysis method is a promising technique for EFES reception pattern analysis. This method lays the foundation for future directional pattern design and high E-Gain design in the future.

Unedited

## Contributors

Zhenke DING did the conceptualization, data curation, formal analysis, investigation, methodology, project administration, validation, and paper writing. Yi LIU did the conceptualization, funding acquisition, investigation, methodology, project administration, resources, supervision, visualization, and paper writing. Bo WU designed the research and gave the resources. Kai YAN and Yi LIN designed the research and validated the result. Ruibing RAN did the investigation, methodology, resources and validation. Yunqi FU did the conceptualization, supervision, and visualization.

## Conflict of interest

All the authors declare that they have no conflict of interest.

## Data availability

The data that support the findings of this study are available from the corresponding author upon reasonable request.

## References

Adams JJ, Genovesi S, Yang B, et al., 2022. Antenna Element Design Using Characteristic Mode Analysis: Insights and research directions. *IEEE Antennas Propag Mag*, 64(2):32-40. https://doi.org/10.1109/MAP.2022.3145718

Anderson DA, Paradis EG, Raithel G, 2018. A vapor-cell atomic sensor for radio-frequency field detection using a polarization-selective field enhancement resonator. *Applied Physics Letters*, 113(7):073501. https://doi.org/10.1063/1.5038550

Anderson DA, Sapiro RE, Raithel G, 2021. A Self-Calibrated SI-Traceable Rydberg Atom-Based Radio Frequency Electric Field Probe and Measurement Instrument. *IEEE Trans Antennas Propagat*, 69(9):5931-5941. https://doi.org/10.1109/TAP.2021.3060540

Bussey LW, Winterburn A, Menchetti M, et al., 2021. Rydberg RF Receiver Operation to Track RF Signal Fading and Frequency Drift. *J Lightwave Technol*, 39(24):7813-7820.
https://doi.org/10.1109/JLT.2021.3098348

Cardman R, Gonçalves LF, Sapiro RE, et al., 2020. Atomic 2D electric field imaging of a Yagi–Uda antenna near-field using a portable Rydberg-atom probe and measurement instrument. *Advanced Optical Technologies*, 9(5):305-312.
https://doi.org/10.1515/aot-2020-0029

Chen Y, Wang CF, 2015. Characteristic Modes: Theory and Applications in Antenna Engineering. John Wiley & Sons, Inc, Hoboken, NJ.
https://doi.org/10.1002/9781119038900

Choi S, Sarabandi K, 2018. A W-Shaped Antenna With Spatial Polarization Variation for Direction Finding. *Antennas Wirel Propag Lett*, 17(12):2429-2433.
https://doi.org/10.1109/LAWP.2018.2877451

Dicandia FA, Genovesi S, 2023. Design of a Transmission-Type Polarization-Insensitive and Angularly Stable Polarization Rotator by Using Characteristic Modes Theory. *IEEE Trans Antennas Propagat*, 71(2):1602-1612.
https://doi.org/10.1109/TAP.2022.3227459

Dixon K, Nickerson K, Booth DW, et al., 2023. Rydberg-Atom-Based Electrometry Using a Self-Heterodyne Frequency-Comb Readout and Preparation Scheme. *Phys Rev Applied*, 19(3):034078.
https://doi.org/10.1103/PhysRevApplied.19.034078

Fan H, Kumar S, Sedlacek J, et al., 2015. Atom based RF electric field sensing. *J Phys B: At Mol Opt Phys*, 48(20):202001.
https://doi.org/10.1088/0953-4075/48/20/202001

Grundmann L, Manteuffel D, 2021. Using Characteristic Modes for Determining the Incident Field in a Scattering Problem. 2021 IEEE International Symposium on Antennas and Propagation and USNC-URSI Radio Science Meeting (APS/URSI), Singapore, Singapore, p.855-856.
https://doi.org/10.1109/APS/URSI47566.2021.9703784

Harrington R, Mautz J, 1971. Theory of characteristic modes for conducting bodies. *IEEE Trans Antennas Propagat*, 19(5):622-628.
https://doi.org/10.1109/TAP.1971.1139999

Harrington RF, 2001. Time-Harmonic Electromagnetic Fields. IEEE Press [u.a.], New York, NY.

Holloway CL, Gordon JA, Schwarzkopf A, et al., 2014. Sub-wavelength imaging and field mapping via electromagnetically induced transparency and Autler-Townes splitting in Rydberg atoms. *Applied Physics Letters*, 104(24):244102.
https://doi.org/10.1063/1.4883635

Holloway CL, Simons MT, Gordon JA, et al., 2019. Detecting and Receiving Phase-Modulated Signals With a Rydberg Atom-Based Receiver. *Antennas Wirel Propag Lett*, 18(9):1853-1857.
https://doi.org/10.1109/LAWP.2019.2931450

Holloway CL, Prajapati N, Artusio-Glimpse AB, et al., 2022. Rydberg atom-based field sensing enhancement using a split-ring resonator. *Applied Physics Letters*, 120(20):204001.
https://doi.org/10.1063/5.0088532

Hu J, Jiao Y, He Y, et al., 2023. Improvement of response bandwidth and sensitivity of Rydberg receiver using multi-channel excitations. *EPJ Quantum Technol*, 10(1):51.
https://doi.org/10.1140/epjqt/s40507-023-00209-7

Huang S, Pan J, Luo Y, 2018. Study on the Relationships between Eigenmodes, Natural Modes, and Characteristic Modes of Perfectly Electric Conducting Bodies. *International Journal of Antennas and Propagation*, 2018:1-13.
https://doi.org/10.1155/2018/8735635

Jiao Y, Han X, Fan J, et al., 2019. Atom-based receiver for amplitude-modulated baseband signals in high-frequency radio communication. *Appl Phys Express*, 12(12):126002.
https://doi.org/10.7567/1882-0786/ab5463

Liu B, Zhang LH, Liu ZK, et al., 2022. Highly Sensitive Measurement of a Megahertz rf Electric Field with a Rydberg-Atom Sensor. *Phys Rev Applied*, 18(1):014045.
https://doi.org/10.1103/PhysRevApplied.18.014045

Manteuffel D, Lin FH, Li T, et al., 2022. Characteristic Mode-Inspired Advanced Multiple Antennas: Intuitive insight into element-, interelement-, and array levels of compact large arrays and metantennas. *IEEE Antennas Propag Mag*, 64(2):49-57.
https://doi.org/10.1109/MAP.2022.3145714

Mao R, Lin Y, Yang K, et al., 2023. A High-Efficiency Fiber-Coupled Rydberg-Atom Integrated Probe and Its Imaging Applications. *Antennas Wirel Propag Lett*, 22(2):352-356.
https://doi.org/10.1109/LAWP.2022.3212057

Meyer DH, Cox KC, Fatemi FK, et al., 2018. Digital communication with Rydberg atoms and amplitude-modulated microwave fields. *Applied Physics Letters*, 112(21):211108.
https://doi.org/10.1063/1.5028357

Ren K, 2022. Direction Finding Using a Single Antenna With Blade Modulation. *Antennas Wirel Propag Lett*, 21(5):873-877.
https://doi.org/10.1109/LAWP.2022.3149871

Robinson AK, Prajapati N, Senic D, et al., 2021. Determining the angle-of-arrival of a radio-frequency source with a Rydberg atom-based sensor. *Applied Physics Letters*, 118(11):114001.
https://doi.org/10.1063/5.0045601

Sandidge G, Santamaria-Botello G, Bottomley E, et al., 2024. Resonant Structures for Sensitivity Enhancement of Rydberg-Atom Microwave Receivers. *IEEE Trans Microwave Theory Techn*, XX:1-10.
https://doi.org/10.1109/TMTT.2024.3355763

Sedlacek JA, Schwettmann A, Kübler H, et al., 2013. Atom-Based Vector Microwave Electrometry Using Rubidium Rydberg Atoms in a Vapor Cell. *Phys Rev Lett*, 111(6):063001.
https://doi.org/10.1103/PhysRevLett.111.063001

Sedlacek JA, Schwettmann A, Kübler H, et al., 2012. Microwave electrometry with Rydberg atoms in a vapour cell using bright atomic resonances. *Nature Phys*, 8(11):819-824.
https://doi.org/10.1038/nphys2423

Shi G, Jia Y, Liu Y, et al., 2023. Theoretic Study of Antenna Scattering Problems Based on Characteristic Modes and

Unedited

its Applications in Reducing Antenna Scattering. *IEEE Trans Antennas Propagat*, 71(3):2098-2109.
https://doi.org/10.1109/TAP.2022.3229174

Simons MT, Artusio-Glimpse AB, Holloway CL, et al., 2021. Continuous radio-frequency electric-field detection through adjacent Rydberg resonance tuning. *Phys Rev A*, 104(3):032824.
https://doi.org/10.1103/PhysRevA.104.032824

Song Z, Liu H, Liu X, et al., 2019. Rydberg-atom-based digital communication using a continuously tunable radio-frequency carrier. *Opt Express*, 27(6):8848.
https://doi.org/10.1364/OE.27.008848

Wu B, Lin Y, Liao D, et al., 2022. Design of locally enhanced electric field in dielectric loaded rectangular resonator for quantum microwave measurements. *Electronics Letters*, 58(24):914-916.
https://doi.org/10.1049/ell2.12618

Wu B, Lin Y, Wu FC, et al., 2023. Quantum microwave electric field measurement technology based on enhancement electric filed resonator. *Acta Phys Sin*, 72(3):034204.
https://doi.org/10.7498/aps.72.20221582

Wu B, Zhou YL, Ding ZK, et al., 2024. Eliminating sensing blind spots of field-enhanced Rydberg atomic antenna via an asymmetric parallel-plate resonator. *EPJ Quantum Technol*, 11(1):30.
https://doi.org/10.1140/epjqt/s40507-024-00239-9

Yang K, Sun Z, Mao R, et al., 2022. Wideband Rydberg atom-based receiver for amplitude modulation radio frequency communication. *Chin Opt Lett*, 20(8):081203.
https://doi.org/10.3788/COL202220.081203

Yang K, Mao R, An Q, et al., 2023a. Amplitude-modulated RF field Rydberg atomic sensor based on homodyne technique. *Sensors and Actuators A: Physical*, 351:114167.
https://doi.org/10.1016/j.sna.2023.114167

Yang K, Mao R, An Q, et al., 2023b. Laser frequency locking method for Rydberg atomic sensing. *Chin Opt Lett*, 21(2):021407.
https://doi.org/10.3788/COL202321.021407

Yang K, Mao R, He L, et al., 2023c. Local oscillator port embedded field enhancement resonator for Rydberg atomic heterodyne technique. *EPJ Quantum Technol*, 10(1):23.
https://doi.org/10.1140/epjqt/s40507-023-00179-w

Yao J, An Q, Zhou Y, et al., 2022. Sensitivity enhancement of far-detuned RF field sensing based on Rydberg atoms dressed by a near-resonant RF field. *Opt Lett*, 47(20):5256.
https://doi.org/10.1364/OL.465048

Yuan S, Jing M, Zhang H, et al., 2024. Isotropic antenna based on Rydberg atoms. *Opt Express*, 32(5):8379.
https://doi.org/10.1364/OE.517149

Zhang D, Chen Y, Yang S, 2022. A Self-Decoupling Method for Antenna Arrays Using High-Order Characteristic Modes. *IEEE Trans Antennas Propagat*, 70(4):2760-2769.
https://doi.org/10.1109/TAP.2021.3125388

Zhang F, Jin B, Lan Z, et al., 2023. Quantum Wireless Sensing: Principle, Design and Implementation. Proceedings of the 29th Annual International Conference on Mobile Computing and Networking, Madrid Spain, p.1-15.
https://doi.org/10.1145/3570361.3613258

Unedited